Science Advances
AAAS

advances.sciencemag.org/cgi/content/full/6/50/eabd1654/DC1

Supplementary Materials for

Overturning circulation, nutrient limitation, and warming in the Glacial North Pacific

J. W. B. Rae*, W. R. Gray, R. C. J. Wills, I. Eisenman, B. Fitzhugh, M. Fotheringham, E. F. M. Littley, P. A. Rafter, R. Rees-Owen, A. Ridgwell, B. Taylor, A. Burke

*Corresponding author. Email: jwbr@st-andrews.ac.uk

Published 9 December 2020, *Sci. Adv.* **6**, eabd1654 (2020)
DOI: 10.1126/sciadv.abd1654

The PDF file includes:

Figs. S1 to S14
Tables S1 and S2
References

Other Supplementary Material for this manuscript includes the following:

(available at advances.sciencemag.org/cgi/content/full/6/50/eabd1654/DC1)

Data file S1

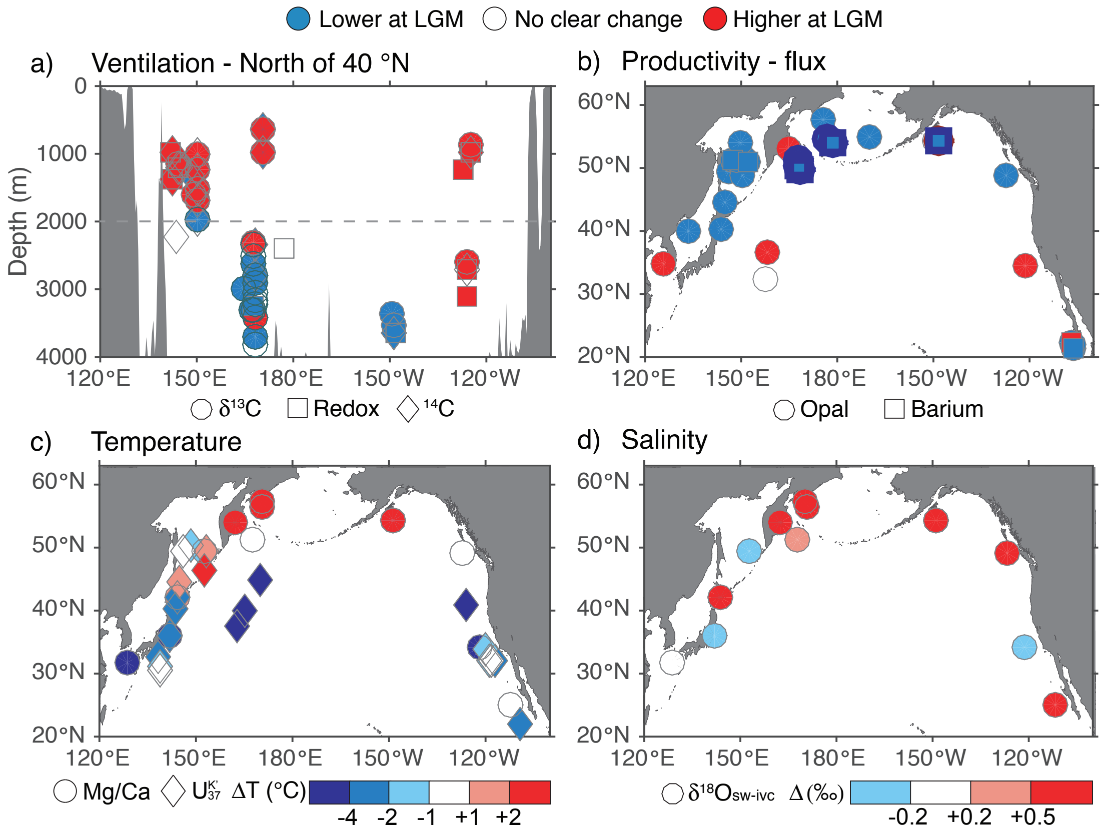

Figure S1: Further detail of changes in ventilation (a), export productivity (b), temperature (c), and salinity (d) at the LGM relative to the Holocene, following Figure 2 in the main text. Red indicates an increase at the LGM relative to the Holocene, blue a decrease, and white no clear change outside of 1σ uncertainty. Ventilation proxies ($\delta^{13}C$, circles; benthic-planktic radiocarbon offsets, diamonds; redox tracers, squares) are shown here only for sites more northerly than 40 °N (c.f. 20 °N in Figure 2). Productivity data (opal, circles; biogenic barium, squares) are shown here as mass accumulation rate of biogenic material into sediment. In most cases this is calculated using $\delta^{18}O$ or ^{14}C derived sediment core age models and dry bulk density, either measured or estimated from the compilation of Kohfeld & Chase (*26*); ^{230}Th-normalisation is used at a subset of sites, indicated with bold symbol outlines. Temperature reconstructions (planktic foraminiferal Mg/Ca, circles; alkenone saturation index $U^{K'}_{37}$, diamonds) and change in salinity ($\delta^{18}O$ on planktic foraminifera corrected for temperature using Mg/Ca and for whole ocean $\delta^{18}O$ and salinity changes due to ice volume) are shown using a graduated scale to illustrate the magnitude of change. This alternative presentation of the data in Figure 2 of the main text supports the conclusion that the subpolar LGM North Pacific was better ventilated at intermediate depths, with lower productivity, and relatively warm and salty surface waters.

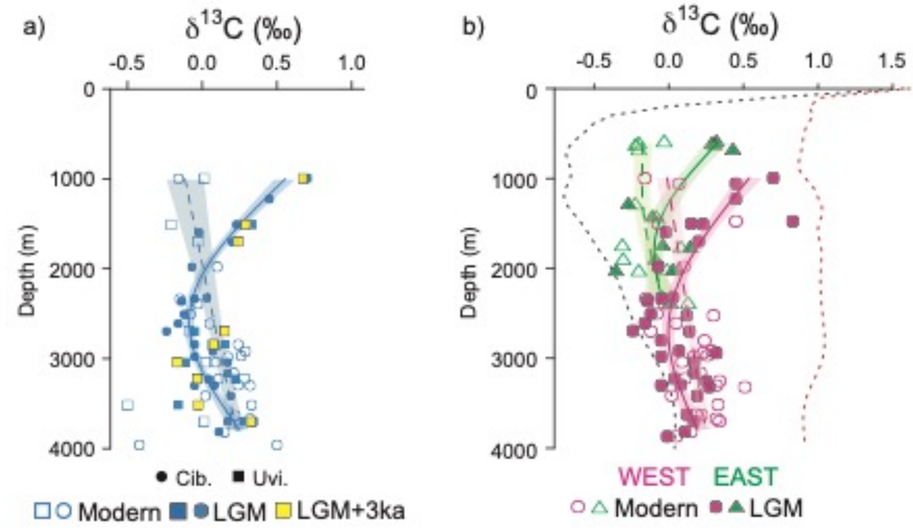

Figure S2: Further detail on δ13C depth profiles, highlighting minimal influence of age model uncertainties (a) and regional differences (b). (a) Benthic foraminiferal δ13C data from the northwest Pacific from the Holocene (open symbols), LGM (closed blue symbols), and a timeslice 3000 years older than the LGM timeslice (closed yellow symbols) (***6***). *Cibicides* spp. are shown in circles, *Uvigerina* in squares; although *Uvigerina* are not typically used for estimates of bottom water δ13C, they are indistinguishable from the *Cibicides* data at the LGM, and allow extension of the profile deeper in time (as *Cibicides* data do not extend beyond the LGM). LGM and LGM+3ka δ13C data have been corrected for a whole ocean δ13C change of 0.34 ‰ (***17***). The LGM and Holocene foraminiferal δ13C are fit with a general additive model. (b) Holocene (open symbols) and LGM (closed symbols) foraminiferal δ13C data from across the basin, as used in the ventilation proxy compilation (see Methods). Data from west of the dateline is shown in pink, east in green, and each profile has been fit with a general additive model. Water column δ13C for the North Pacific (black dotted line) and North Atlantic (red dotted line) are taken from the recent compilation of (***162***), and include all values between 40-65 °N in each basin; here a generalized additive model fit to the data is shown. The Pacific depth profile of δ13C is notably different at the LGM, with elevated values found at intermediate depths. The glacial increase in intermediate depth δ13C is more apparent in the west of the basin relative to the east; this is suggestive of a source of local ventilation in west of the basin.

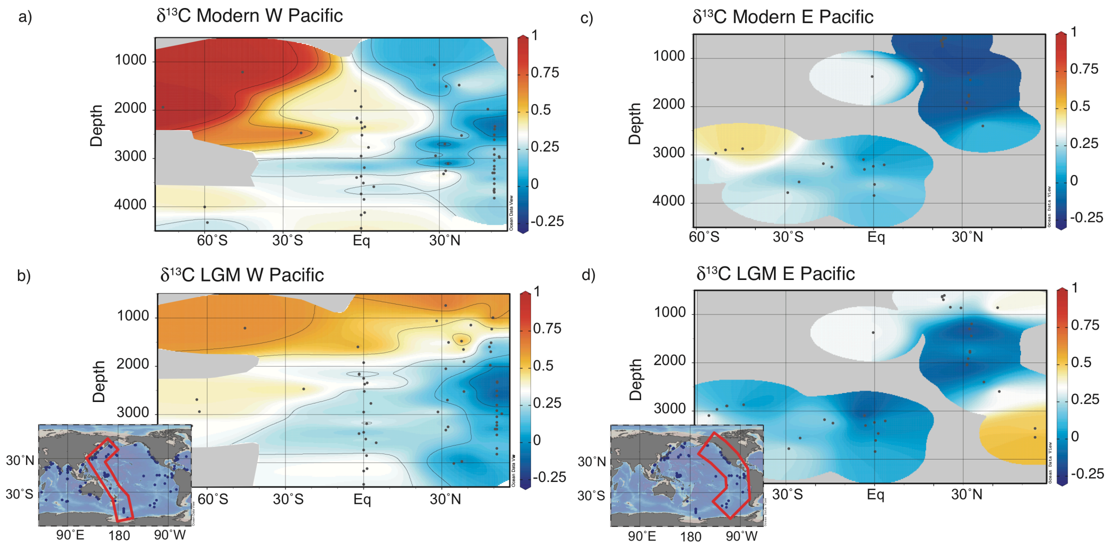

Figure S3: Meridional δ^{13}C sections from benthic foraminifera in the Western (a, b) and Eastern (c, d) Pacific in the late Holocene (a, c) and at the LGM (b, d). Data are taken from the compilation of (*17*), with glacial data corrected for a whole ocean δ^{13}C change of 0.34 ‰, and are plotted using Ocean Data View (*54*). The location of the data making up these sections are shown in the inset maps. Areas of poor data coverage are shown in grey. At the LGM there is a substantial increase in δ^{13}C of intermediate waters in the North Pacific, indicating enhanced ventilation. The largest change is observed in the West of the basin, as expected from the formation of a deep western boundary current.

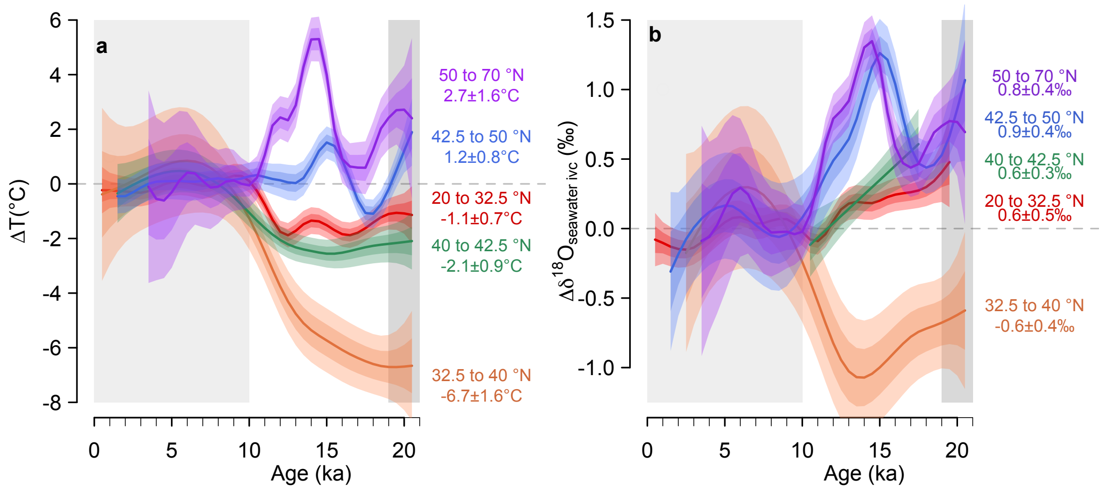

Figure S4: Latitudinally binned deglacial changes in SST (a) and δ^{18}O of seawater (b). (a) At each site Mg/Ca and/or $U^{K'}_{37}$ SSTs were converted to a difference from Holocene (0-10 ka, light grey box) and binned by latitude. (b) δ^{18}O of seawater, derived from paired measurements of Mg/Ca and $\delta^{18}O_{calcite}$ and corrected for changes in global ice volume, was converted to a difference from Holocene and binned by latitude. The latitudinally binned SST and $\delta^{18}O_{seawater}$ data were modelled as a function of time using a generalised additive model (GAM), with the 68% and 95% Bayesian credible intervals shown (*161*, *163*). For each latitudinal SST and $\delta^{18}O_{seawater}$ bin, the LGM (19-21 ka, dark grey box) value is given with the 95% confidence interval.

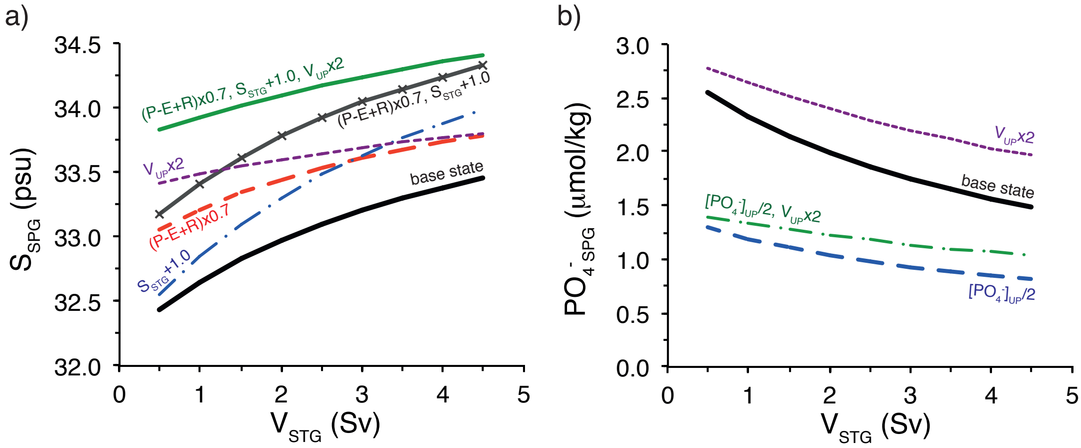

Figure S5: Model sensitivity tests, showing the salinity (a) and phosphate concentration (b) of surface waters in the subpolar North Pacific, as a function of exchange with the subtropical gyre (V_{STG}) under different boundary conditions. Base state values are given in Table S2; P-E+R is net precipitation plus riverine run-off; S_{STG} is the salinity of the subtropical gyre; V_{UP} is the upwelling flux; $[PO_4^-]_{UP}$ is the phosphate concentration of upwelled water. Subpolar salinity increases when (i) net precipitation is reduced, (ii) upwelling is increased, and (iii) exchange with the subtropics is enhanced, particularly when subtropical salinity is elevated. Phosphate concentrations in the subpolar gyre are reduced by exchange with the subtropics and by decreasing the phosphate concentrations of upwelled waters, and are increased by increasing the upwelling flux. Note that the net effect of doubling vertical exchange while halving subsurface nutrients is similar to that of halving subsurface nutrients alone. Because the wind- and tidally-driven transfer of water from the subsurface to the surface North Pacific is high vertical nutrient gradients are relatively low, so further increase in vertical exchange – for instance due to convective mixing – has less influence than decreasing the nutrient content of the upwelled water.

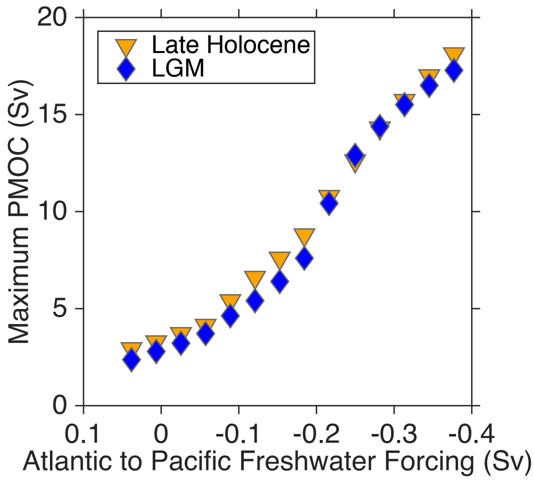

Figure S6: The relationship between Atlantic to Pacific freshwater forcing and maximum PMOC in cGENIE. Forcing values are shown as anomalies relative to the prescribed Atlantic to Pacific freshwater flux, which has a default value of 0.23 Sv (i.e. the default flux of 0.23 Sv plots as 0 on the figure above).

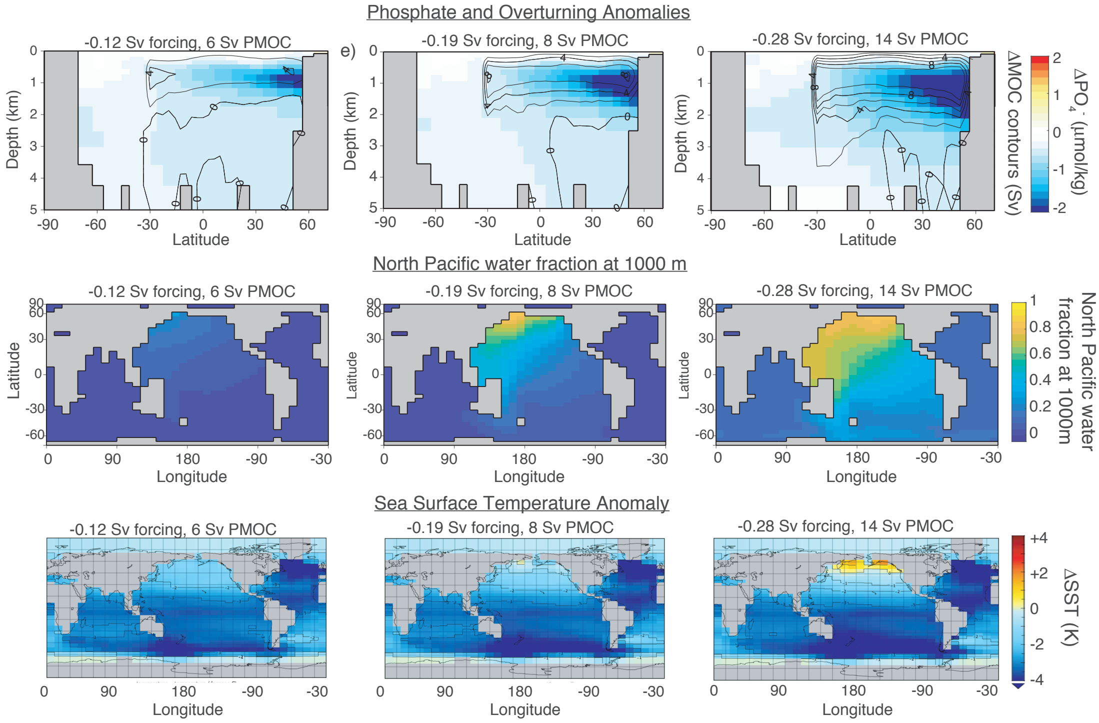

Figure S7: Representative cGENIE experiments spanning a range of PMOC states. Top row shows phosphate and overturning anomalies, illustrating the flushing of phosphate from the upper reaches of the North Pacific as overturning increases. Bottom row shows the North Pacific water fraction at 1000 m, based on a dye tracer tagging surface waters north of 40 °N in the North Pacific. These experiments were run under glacial boundary conditions. Newly formed NPIW travels south as a western boundary current, while the eastern basin feels relatively little influence of NPIW at low latitudes. Even at high overturning rates, North Pacific deep water is largely confined to the Pacific basin. Note that the central experiment (-0.19 Sv forcing and 8 Sv PMOC) shows the best fit to the data in Figures 5, S10.

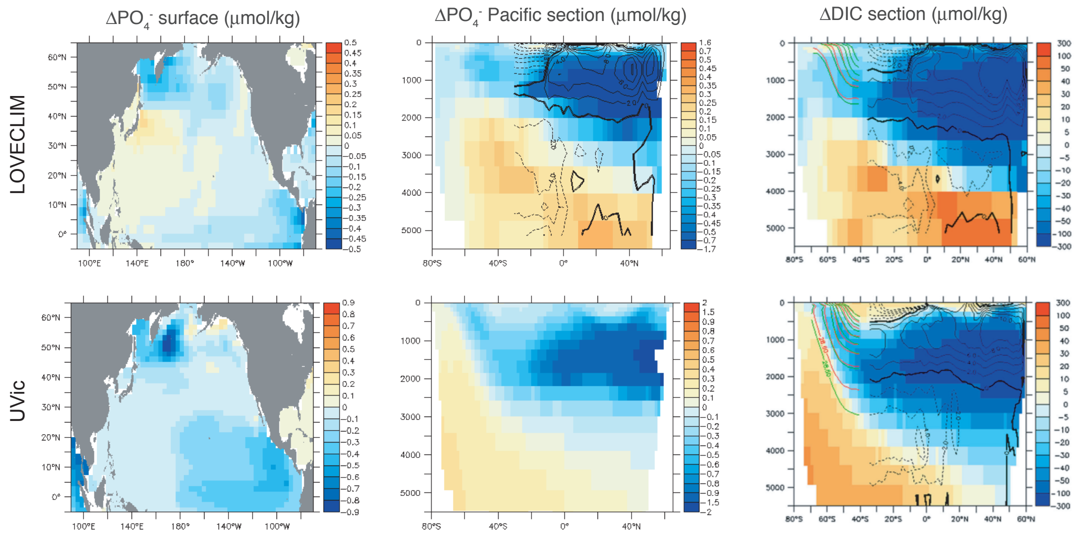

Figure S8: Phosphate and Dissolved Inorganic Carbon (DIC) anomalies under enhanced PMOC in simulations with the LOVECLIM (1.1) and UVic (v2.9) Earth System Models by Menviel et al.(*28*). These simulations were forced with North Atlantic freshwater hosing of 0.1 Sv for 2000 years (fNA in the rubric of the original publication), which produces a strong PMOC in response (stream function contours are shown for LOVECLIM). As in cGENIE, the establishment of an active overturning circulation in these higher resolution models flushes nutrients from the upper reaches of the North Pacific.

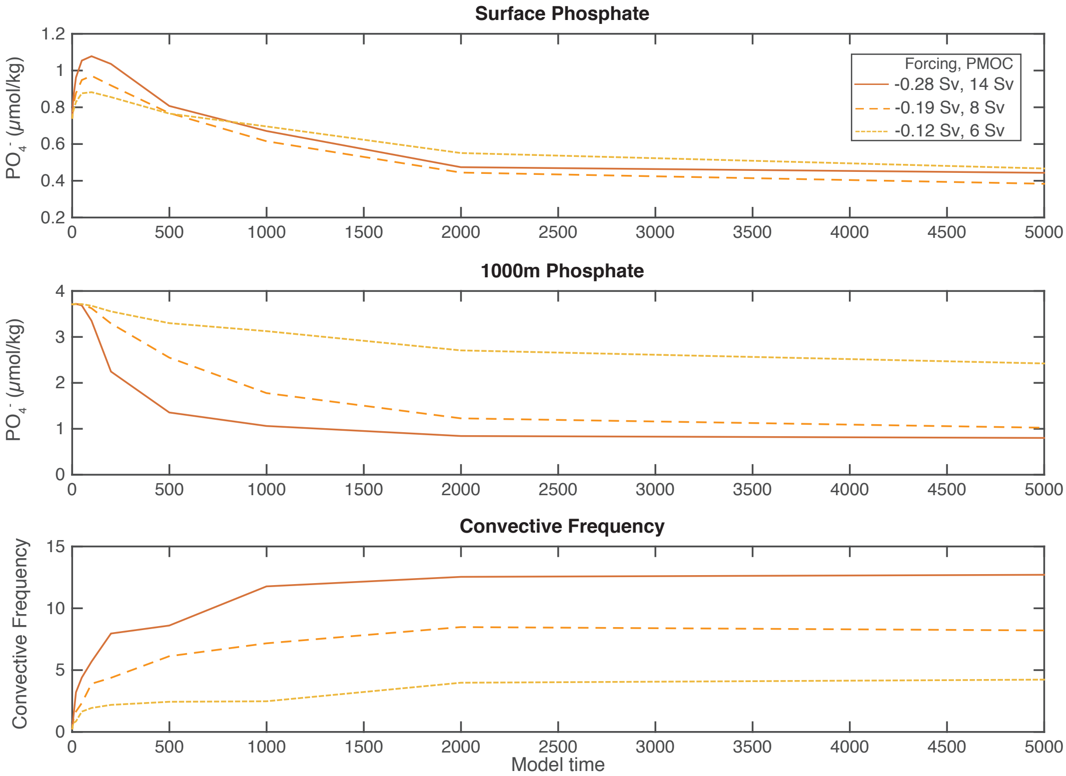

Figure S9: Transient response of North Pacific surface nutrients at the onset of enhanced overturning in cGENIE. Data are shown for the NW of the subpolar gyre in simulations spanning a range of overturning states (as in Figure S7). For the first several hundred years after North Pacific salinity is increased, surface phosphate shows a transient increase (top panel), as convective mixing increases (bottom panel) and subsurface nutrients remain relatively high (middle panel). As overturning becomes established, nutrient-rich subsurface waters are flushed out, reducing surface nutrient supply despite the increase in convective mixing, as described in main text (e.g. Figure 4).

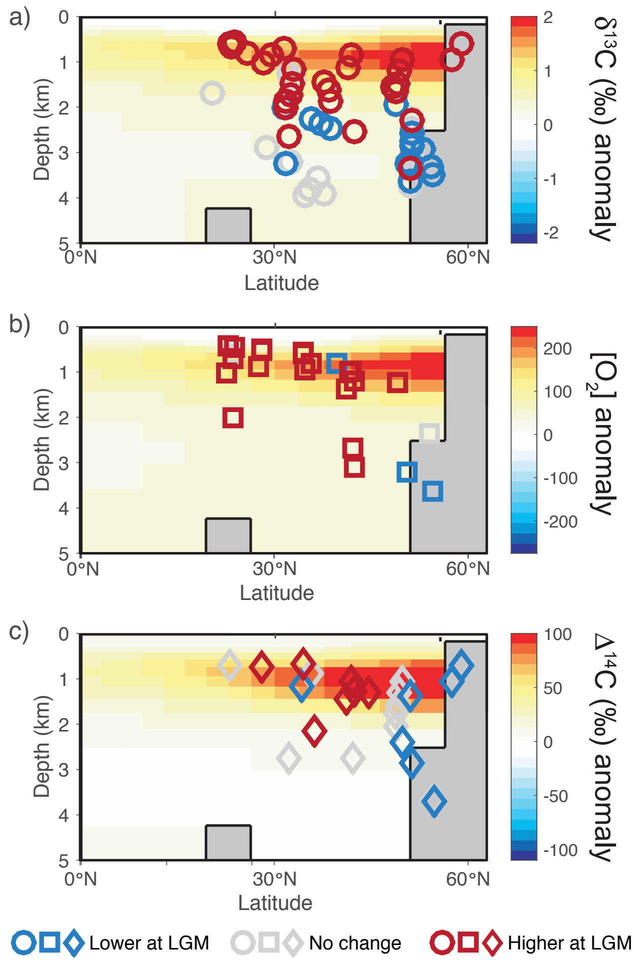

Figure S10: Simulated changes in δ^{13}C (a), oxygen concentration (b), and Δ^{14}C (c) compared to the changes seen in our LGM data compilation. The simulated section is from 165 °W for the experiment run with an Atlantic to Pacific freshwater forcing of -0.18 Sv under glacial boundary conditions and is shown as an anomaly from conditions prior to anomalous salinity forcing. This experiment shows the best match to LGM δ^{13}C profile data (Figure 5). Note that as the abyssal Pacific likely remains ventilated by Southern Ocean waters at depths greater than 2000 m, and as we have not made any changes to the Southern Ocean in our simulations, some offsets between the experiments and the data are to be expected at depth.

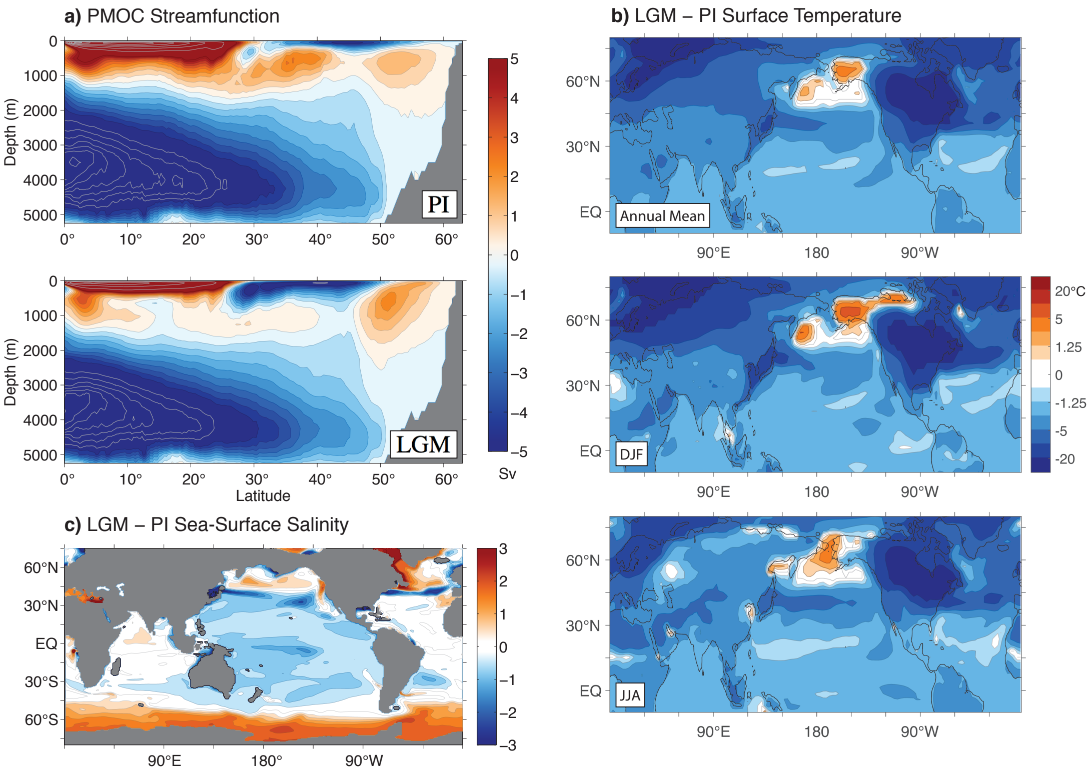

Figure S11: Annual mean meridional overturning circulation streamfunction (a), surface temperature (b), and sea surface salinity (c) in the North Pacific in simulations of preindustrial and LGM climate with the Community Climate System Model version 3 (CCSM3). The North Pacific streamfunction is diagnosed from the difference between the Eulerian mean streamfunction of the global ocean and the Atlantic, both of which are output directly from the model. Positive values denote a clockwise circulation. Preindustrial properties are averaged over model years 470-489 of the preindustrial control simulation described by Otto-Bliesner et al.(*164*), and LGM properties over model years 380-399 of the simulation described by Otto-Bliesner et al.(*164, 165*). LGM conditions include greenhouse gas forcings and insolation at 21 ka values, and ice sheets based on the 21 ka reconstruction from ICE-5G (*166*). Note the enhanced intermediate-depth overturning, warming of NW Pacific waters, and increased salinity of surface waters in the North Pacific under glacial conditions.

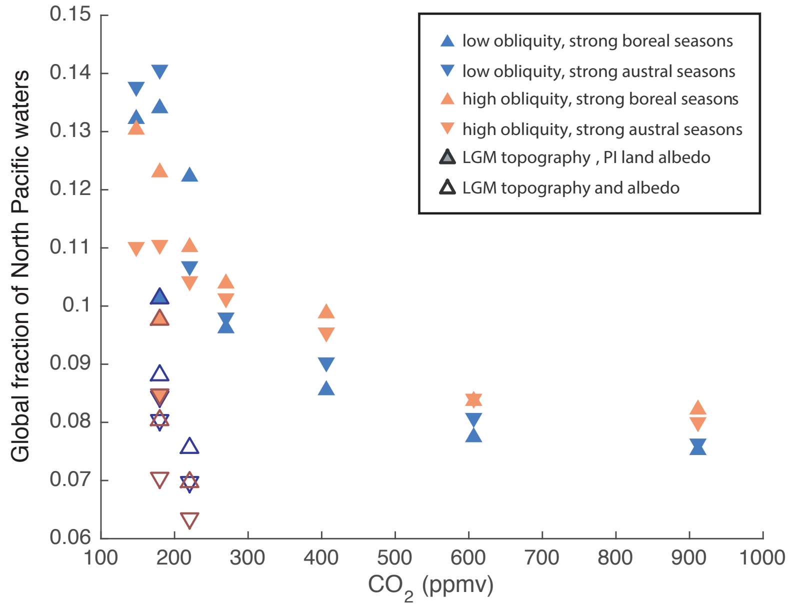

Figure S12: Volumetric contribution of North Pacific waters to the global ocean in the CM2Mc model under a range of boundary conditions. Simulations are from (*167*) and were designed to ensure equilibration of the deep ocean. North Pacific waters were tagged using a tracer in surface waters >30 °N in the Pacific basin. The fraction of North Pacific waters filling the global ocean systematically increases with decreasing CO_2, supporting the idea that a colder climate enhances the formation of NPIW. We note that in these simulations NPIW formation is decreased in the presence of LGM ice sheets, although the geometry of the ice sheets used in these simulations is now thought to have some significant inaccuracies compared to more recent reconstructions (*168*). CM2Mc also has a cold bias in the North Pacific, which leads to relatively high NPIW formation under modern conditions (*167*). Nevertheless, these simulations illustrate the potential for enhanced North Pacific overturning in a state-of-the-art Earth system model under cold climate conditions.

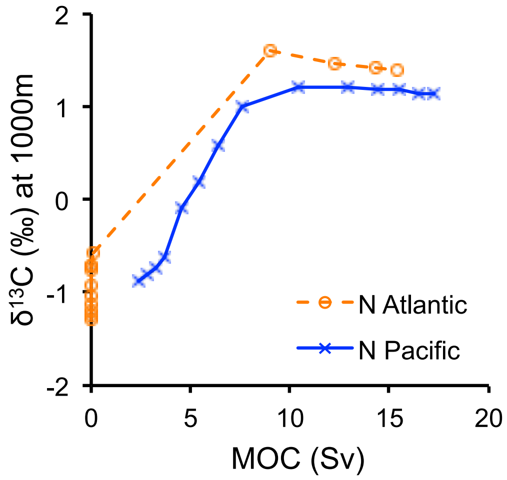

Figure S13: Intermediate water $\delta^{13}C$ from cGENIE over a range of overturning states in the North Atlantic (orange circles and dashed line) and North Pacific (blue crosses and solid line). Values are taken from 1000 m at a central position in each Northern basin (40 °N 165 °W in the Pacific, 48 °N 35 °W in the Atlantic). Intermediate depth $\delta^{13}C$ is consistently lower in the North Pacific than in the North Atlantic under similar rates of overturning.

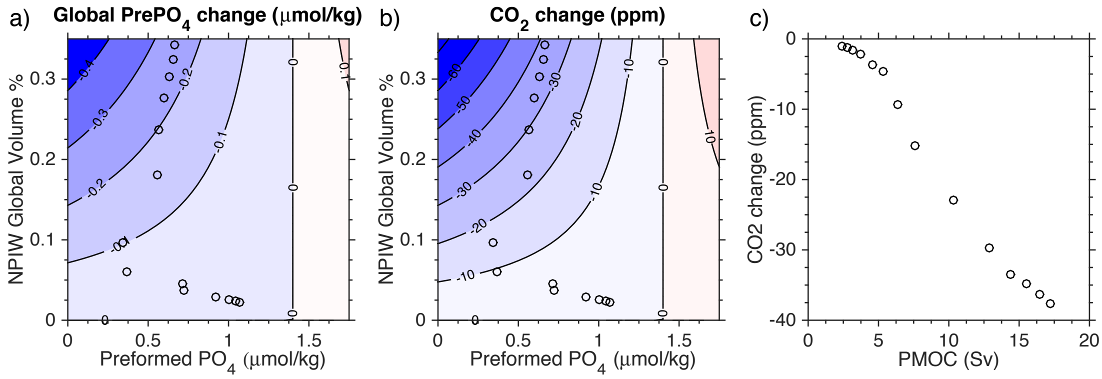

Figure S14: Change in the inventory of preformed phosphate (a) and atmospheric CO_2 (b) as a function of changes in NPIW's global volume fraction, preformed phosphate composition, and PMOC (c). Shaded contours show the result of mass balance calculations, assuming NPIW replaces water with preformed phosphate of 1.4 (*158*), with CO_2 change then calculated using the scaling of Ito & Follows (*33*). Symbols in (a) and (b) show the NPIW volume and preformed phosphate found in our cGENIE experiments, and (c) shows the calculated change in CO_2 using these values and the scaling of (*33*) against the maximum PMOC for each experiment. Note the sensitivity of CO_2 to changes in PMOC of ~6-12 Sv (c), driven by the increase in the volume of the global ocean occupied by NIPW (b).

	Model inputs				Model outputs	
	P-E + R	S_{STG}	V_{STG}	$PO_4^-{}_{UP}$	S_{SPG}	$PO_4^-{}_{SPG}$
	Sv	psu	Sv	μmol/kg	psu	μmol/kg
Modern Pacific - observed	0.21 + 0.07	34.6	2	3.1	33.0	1.8
Modern Pacific - model	0.21 + 0.07	34.6	2	3.1	33.0	2.0
Subtropical salinity + 1 psu	0.21 + 0.07	35.6	2	3.1	33.3	2.0
Gyre exchange + 2 Sv	0.21 + 0.07	34.6	4	3.1	33.4	1.6
Subtropical salinity & Gyre exchange combined	0.21 + 0.07	35.6	4	3.1	33.9	1.6
Net rainfall (P-E) - 30%	0.15 + 0.05	34.6	2	3.1	33.7	2.0
Subtropical salinity, Gyre exchange, P-E combined	0.15 + 0.05	35.6	4	3.1	34.2	1.6
As above with 2x upwelling & 0.5x upwelled [PO_4]	0.15 + 0.05	35.6	4	1.5	34.4	1.1
Modern Atlantic - observed	0.10 + 0.06	36.6	5-10	1.1	35.0	0.8

Table S1:

Results of calculations based on Warren's box model. Input values include net precipitation (P-E) and riverine runoff (R), the salinity of the subtropical gyre (S_{STG}), advection from the subtropical gyre (V_{STG}), and the phosphate concentration of upwelled waters (PO_{4UP}). Output values are the salinity (S_{SPG}) and phosphate concentration (PO_{4SPG}) of the top 200 m of the subpolar gyre.

P-E	R	V_{STG}	V_{UP}	S_{STG}	S_{UP}	$PO_4^-{}_{STG}$	$PO_4^-{}_{UP}$
Sv	Sv	Sv	Sv	psu	Sv	μmol/kg	μmol/kg
0.213	0.07	2.02	3.74	34.6	34.6	0.28	3.1

Table S2:

Model input parameters for modern base state. P-E and R are from ERA-Interim reanalysis from (*148*), V_{STG} and V_{UP} are from (*3*) and salinity and phosphate concentrations are from World Ocean Atlas, computed using the box averaging tool in Ocean Data View (*149*).

REFERENCES AND NOTES

1. D. M. Sigman, M. P. Hain, G. H. Haug, The polar ocean and glacial cycles in atmospheric CO2 concentration. *Nature* **466**, 47–55 (2010).
2. B. A. Warren, Why is no deep water formed in the North Pacific? *J. Mar. Res.* **41**, 327–347 (1983).
3. J. Emile-Geay, M. A. Cane, N. Naik, R. Seager, A. C. Clement, A. van Geen, Warren revisited: Atmospheric freshwater fluxes and "why is no deep water formed in the North Pacific". *J. Geophys. Res.* **108**, 3178 (2003).
4. D. Ferreira, P. Cessi, H. K. Coxall, A. de Boer, H. A. Dijkstra, S. S. Drijfhout, T. Eldevik, N. Harnik, J. F. McManus, D. P. Marshall, J. Nilsson, F. Roquet, T. Schneider, R. C. Wills, Atlantic-Pacific asymmetry in deep water formation. *Annu. Rev. Earth Planet. Sci.* **46**, 327–352 (2018).
5. J. L. Sarmiento, N. Gruber, M. A. Brezinski, J. P. Dunne, High-latitude controls of thermocline nutrients and low latitude biological productivity. *Nature* **427**, 56–60 (2004).
6. L. D. Keigwin, Glacial-age hydrography of the far northwest Pacific Ocean. *Paleoceanography* **13**, 323–339 (1998).
7. S. L. Jaccard, E. D. Galbraith, Large climate-driven changes of oceanic oxygen concentrations during the last deglaciation. *Nat. Geosci.* **5**, 151–156 (2011).
8. K. P. Knudson, A. C. Ravelo, North Pacific Intermediate Water circulation enhanced by the closure of the Bering Strait. *Paleoceanography* **30**, 1287–1304 (2015).
9. L. Max, N. Rippert, L. Lembke-Jene, A. Mackensen, D. Nürnberg, R. Tiedemann, Evidence for enhanced convection of North Pacific Intermediate Water to the low-latitude Pacific under glacial conditions. *Paleoceanography* **32**, 41–55 (2016).
10. M. S. Cook, A. C. Ravelo, A. Mix, I. M. Nesbitt, N. V. Miller, Tracing subarctic Pacific water masses with benthic foraminiferal stable isotopes during the LGM and late Pleistocene. *Deep Sea Res. II Topical Stud. Ocean.* **125–126**, 84–95 (2016).
11. K. Matsumoto, T. Oba, J. Lynch-Stieglitz, H. Yamamoto, Interior hydrography and circulation of the glacial Pacific Ocean. *Quat. Sci. Rev.* **21**, 1693–1704 (2002).
12. J. W. B. Rae, M. Sarnthein, G. L. Forster, A. Ridgwell, P. M. Grootes, T. Elliot, Deep water formation in the North Pacific and deglacial CO_2 rise. *Paleoceanography* **29**, 645–667 (2014).
13. Y. Okazaki, A. Timmermann, L. Menviel, N. Harada, A. Abe-Ouchi, M. O. Chikamoto, A. Mouchet, H. Asahi, Deepwater formation in the North Pacific during the last glacial termination. **329**, 200–204 (2010).

14. D. M. Sigman, S. L. Jaccard, G. H. Haug, Polar ocean stratification in a cold climate. *Nature* **428**, 59–63 (2004).
15. H. Ren, A. S. Studer, S. Serno, D. M. Sigman, Glacial-to-interglacial changes in nitrate supply and consumption in the subarctic North Pacific from microfossil-bound N isotopes at two trophic levels. *Biogeosciences* **30**, 1217–1232 (2015).
16. E. Tamm, T. Kivisild, M. Reidla, M. Metspalu, D. G. Smith, C. J. Mulligan, C. M. Bravi, O. Rickards, C. Martinez-Labarga, E. K. Khusnutdinova, S. A. Fedorova, M. V. Golubenko, V. A. Stepanov, M. A. Gubina, S. I. Zhadanov, L. P. Ossipova, L. Damba, M. I. Voevoda, J. E. Dipierri, R. Villems, R. S. Malhi, Beringian standstill and spread of Native American founders. *PLOS ONE* **2**, e829–6 (2007).
17. C. D. Peterson, L. E. Lisiecki, J. V. Stern, Deglacial whole-ocean $\delta^{13}C$ change estimated from 480 benthic foraminiferal records. *Paleoceanography* **29**, 549–563 (2014).
18. N. Zhao, O. Marchal, L. Keigwin, D. Amrhein, G. Gebbie, A synthesis of deglacial deep-sea radiocarbon records and their (In)Consistency with modern ocean ventilation. *Paleoceanogr. Paleoclimatol.* **33**, 128–151 (2018).
19. L. C. Skinner, F. Primeau, E. Freeman, M. de la Fuente, P. A. Goodwin, J. Gottschalk, E. Huang, I. N. McCave, T. L. Noble, A. E. Scrivner, Radiocarbon constraints on the glacial ocean circulation and its impact on atmospheric CO_2. *Nat. Commun.* **8**, 16010 (2017).
20. L. D. Keigwin, S. J. Lehman, Radiocarbon evidence for a possible abyssal front near 3.1 km in the glacial equatorial Pacific Ocean. **425**, 93–104 (2015).
21. D. C. Lund, J. F. Adkins, R. Ferrari, Abyssal Atlantic circulation during the Last Glacial Maximum: Constraining the ratio between transport and vertical mixing. *Paleoceanography* **26**, PA1213 (2011).
22. W. R. Gray, R. C. J. Wills, J. W. B. Rae, A. Burke, R. F. Ivanovic, W. H. G. Roberts, D. Ferreira, P. J. Valdes, Wind-driven evolution of the north pacific subpolar gyre over the last deglaciation. *Geophys. Res. Lett.* **47**, 208–12 (2020).
23. N. Harada, O. Seki, A. Timmermann, H. Moossen, J. Bendle, Y. Nakamura, K. Kimoto, Y. Okazaki, K. Nagashima, S. A. Gorbarenko, A. Ijiri, T. Nakatsuka, L. Menviel, M. O. Chikamoto, A. Abe-Ouchi, S. Schouten, Sea surface temperature changes in the Okhotsk Sea and adjacent North Pacific during the last glacial maximum and deglaciation. *Deep Sea Res. II Top. Stud. Oceanogr.* **61-64**, 93–105 (2012).

24. J.-R. Riethdorf, L. Max, D. Nürnberg, L. Lembke-Jene, R. Tiedemann, Deglacial development of (sub) sea surface temperature and salinity in the subarctic northwest Pacific: Implications for upper-ocean stratification. *Paleoceanography* **28**, 91–104 (2013).
25. M. Méheust, R. Stein, K. Fahl, R. Gersonde, Sea-ice variability in the subarctic North Pacific and adjacent Bering Sea during the past 25 ka: New insights from IP_{25} and $U^{k'}_{37}$ proxy records. *Ark. Dent.* **4**, 1–19 (2018).
26. K. E. Kohfeld, Z. Chase, Controls on deglacial changes in biogenic fluxes in the North Pacific Ocean. *Quat. Sci. Rev.* **30**, 3350–3363 (2011).
27. S. Serno, G. Winckler, R. F. Anderson, E. Maier, H. Ren, R. Gersonde, G. H. Haug, Comparing dust flux records from the Subarctic North Pacific and Greenland: Implications for atmospheric transport to Greenland and for the application of dust as a chronostratigraphic tool. *Paleoceanography* **30**, 583–600 (2015).
28. L. Menviel, M. H. England, K. J. Meissner, A. Mouchet, J. Yu, Atlantic-Pacific seesaw and its role in outgassing CO_2 during Heinrich events. *Paleoceanography* **29**, 58–70 (2014).
29. W. R. Gray, J. W. B. Rae, R. C. J. Wills, A. E. Shevenell, B. Taylor, A. Burke, G. L. Foster, C. H. Lear, Deglacial upwelling, productivity and CO_2 outgassing in the North Pacific Ocean. *Nat. Geosci.* **11**, 340–344 (2018).
30. I. M. Held, B. J. Soden, Robust responses of the hydrological cycle to global warming. *J. Climate* **19**, 5686–5699 (2006).
31. J. M. Lora, J. L. Mitchell, A. E. Tripati, Abrupt reorganization of North Pacific and western North American climate during the last deglaciation. *Geophys. Res. Lett.* **43**, 11796–11804 (2016).
32. H. Stommel, Thermohaline convection with two stable regimes of flow. *Tellus* **13**, 224–230 (1961).
33. T. Ito, M. J. Follows, Preformed phosphate, soft tissue pump and atmospheric CO_2. *J. Mar. Res.* **63**, 813–839 (2005).
34. M. P. Hain, D. M. Sigman, G. H. Haug, Carbon dioxide effects of Antarctic stratification, North Atlantic Intermediate Water formation, and subantarctic nutrient drawdown during the last ice age: Diagnosis and synthesis in a geochemical box model. *Global Biogeochem. Cycles* **24**, GB4023 (2010).
35. G. H. Haug, D. M. Sigman, Palaeoceanography: Polar twins. *Nat. Geosci.* **2**, 91–92 (2009).
36. K. E. Graf, I. Buvit, Human dispersal from Siberia to Beringia: Assessing a Beringian standstill in light of the archaeological evidence. *Curr. Anthropol.* **58**, S583–S603 (2017).

37. V. D. Meyer, J. Hefter, G. Lohmann, L. Max, R. Tiedemann, G. Mollenhauer, Summer temperature evolution on the Kamchatka Peninsula, Russian Far East, during the past 20 000 years. *Clim. Past* **13**, 359–377 (2017).
38. M. Melles, J. Brigham-Grette, P. S. Minyuk, N. R. Nowaczyk, V. Wennrich, R. M. DeConto, P. M. Anderson, A. A. Andreev, A. Coletti, T. L. Cook, E. Haltia-Hovi, M. Kukkonen, A. V. Lozhkin, P. Rosén, P. Tarasov, H. Vogel, B. Wagner, 2.8 million years of Arctic climate change from Lake El'gygytgyn, NE Russia. *Science* **337**, 315–320 (2012).
39. J. C. Herguera, T. Herbert, M. Kashgarian, C. Charles, Intermediate and deep water mass distribution in the Pacific during the Last Glacial Maximum inferred from oxygen and carbon stable isotopes. *Quat. Sci. Rev.* **29**, 1228–1245 (2010).
40. J. Lynch-Stieglitz, R. G. Fairbanks, C. D. Charles, Glacial-interglacial history of Antarctic Intermediate Water: Relative strengths of Antarctic versus Indian Ocean sources. *Paleoceanography* **9**, 7–29 (1994).
41. L. D. Stott, M. Neumann, D. Hammond, Intermediate water ventilation on the Northeastern Pacific Margin during the Late Pleistocene inferred from benthic foraminiferal $\delta^{13}C$. *Paleoceanography* **15**, 161–169 (2000).
42. J.-C. Duplessy, N. J. Shackleton, R. K. Matthews, W. Prell, W. F. Ruddiman, M. Caralp, C. H. Hendy, ^{13}C Record of benthic foraminifera in the last interglacial ocean: Implications for the carbon cycle and the global deep water circulation. *Quatern. Res.* **21**, 225–243 (1984).
43. D. H. Andreasen, M. Flower, M. Harvey, S. Chang, A. C. Ravelo, Data report: Late Pleistocene oxygen and carbon isotopic records from sites 1011, 1012, and 1018. *Proc. ODP Sci. Results* **167**, 141–144 (2000).
44. E. A. Boyle, Cadmium and $\delta^{13}C$ paleochemical ocean distributions during the stage 2 glacial maximum. *Annu. Rev. Earth Planet. Sci.* **20**, 245–287 (1992).
45. T. Oba, M. Murayama, M. Yamauchi, M. Yamane, S. Oka, H. Yamamoto, Oxygen isotopic ratio of foraminiferal tests in marine sediment cores collected during "Mirai" MR97-04 cruise. *JAMSTEC-R* (1999).
46. M. Lyle, I. Koizumi, C. Richter, R. J. Behl, P. Boden, J.-P. Caulet, M. L. Delaney, P. deMenocal, M. Desmet, E. Fornaciari, A. Hayashida, F. Heider, J. Hood, S. A. Hovan, T. R. Janecek, A. G. Janik, J. Kennett, D. Lund, M. L. Machain C., T. Maruyama, R. B. Merrill, D. J. Mossman, J. Pike, A. C. Ravelo, G. A. Rozo Vera, R. Stax, R. Tada, J. Thurow, M. Yamamoto, Sites 1010 and 1011, in

Proceedings of the Ocean Drilling Program, Initial Reports, R. N. Riegel, Ed. (Ocean Drilling Program, 1997), vol. 167, pp. 49–173.
47. C. Sancetta, M. Lyle, L. Heusser, R. Zahn, J. P. Bradbury, Late-glacial to holocene changes in winds, upwelling, and seasonal production of the northern California current system. *Quatern. Res.* **38**, 359–370 (1992).
48. University of Cambridge, "Delphi", https://www.esc.cam.ac.uk/images/research-images/research-group/research-projects/delphi.
49. L. Wang, M. Sarnthein, H. Erlenkeuser, J. Grimalt, P. Grootes, S. Heilig, E. Ivanova, M. Kienast, C. Pelejero, U. Pflaumann, East Asian monsoon climate during the Late Pleistocene: High-resolution sediment records from the South China Sea. *Mar. Geol.* **156**, 245–284 (1999).
50. S. A. Hovan, D. K. Rea, N. G. Pisias, Late Pleistocene continental climate and oceanic variability recorded in northwest Pacific sediments. *Paleoceanography* **6**, 349–370 (1991).
51. R. Zahn, A. Rushdi, N. G. Pisias, B. D. Bornhold, B. Blaise, R. Karlin, Carbonate deposition and benthic $\delta^{13}C$ in the subarctic Pacific: Implications for changes of the oceanic carbonate system during the past 750,000 years. *Earth Planet. Sci. Lett.* **103**, 116–132 (1991).
52. T. Suzuki, M. Ishii, M. Aoyama, J. R. Christian, K. Enyo, T. Kawano, R. M. Key, N. Kosugi, A. Kozyr, L. A. Miller, A. Murata, T. Nakano, T. Ono, T. Saino, K.-i. Sasaki, D. Sasano, Y. Takatani, M. Wakita, C. L. Sabine, PACIFICA Data Synthesis Project. (ORNL/CDIAC-159, 2013); 10.3334/CDIAC/OTG.PACIFICA_NDP092.
53. L. Max, L. Lembke-Jene, J.-R. Riethdorf, R. Tiedemann, D. Nürnberg, H. Kühn, A. Mackensen, Pulses of enhanced North Pacific Intermediate Water ventilation from the Okhotsk Sea and Bering Sea during the last deglaciation. *Clim. Past* **10**, 591–605 (2014).
54. R. Schlitzer, Ocean Data View (2010); http://odv.awi.de.
55. K. G. Cannariato, J. P. Kennett, Climatically related millennial-scale fluctuations in strength of California margin oxygen-minimum zone during the past 60 k.y. *Geology* **27**, 975–978 (1999).
56. T. S. Ivanochko, T. F. Pedersen, Determining the influences of Late Quaternary ventilation and productivity variations on Santa Barbara Basin sedimentary oxygenation: A multi-proxy approach. *Quat. Sci. Rev.* **23**, 467–480 (2004).
57. I. L. Hendy, T. F. Pedersen, Is pore water oxygen content decoupled from productivity on the California Margin? Trace element results from Ocean Drilling Program Hole 1017E, San Lucia slope, California. **20**, PA4026 (2005).

58. W. E. Dean, Sediment geochemical records of productivity and oxygen depletion along the margin of western North America during the past 60,000 years: Teleconnections with Greenland Ice and the Cariaco Basin. *Quat. Sci. Rev.* **26**, 98–114 (2007).
59. A. S. Chang, T. F. Pedersen, I. L. Hendy, Late Quaternary paleoproductivity history on the Vancouver Island margin, western Canada: A multiproxy geochemical study. *Can. J. Earth Sci.* **45**, 1283–1297 (2008).
60. Y. Zheng, A. van Geen, R. F. Anderson, J. V. Gardner, W. E. Dean, Intensification of the northeast Pacific oxygen minimum zone during the Bölling-Alleröd warm period. *Paleoceanography* **15**, 528–536 (2000).
61. R. S. Ganeshram, T. F. Pedersen, S. E. Calvert, G. W. McNeill, M. R. Fontugne, Glacial-interglacial variability in denitrification in the world's oceans: Causes and consequences. *Paleoceanography* **15**, 361–376 (2000).
62. T. J. Nameroff, S. E. Calvert, J. W. Murray, Glacial-interglacial variability in the eastern tropical North Pacific oxygen minimum zone recorded by redox-sensitive trace metals. *Paleoceanography* **19**, PA1010 (2004).
63. R. J. Behl, J. P. Kennett, Brief interstadial events in the Santa Barbara basin, NE Pacific, during the past 60 kyr. *Nature* **379**, 243–246 (1996).
64. K. G. Cannariato, J. P. Kennett, R. J. Behl, Biotic response to late Quaternary rapid climate switches in Santa Barbara Basin: Ecological and evolutionary implications. *Geology* **27**, 63–66 (1999).
65. E. Emmer, R. C. Thunell, Nitrogen isotope variations in Santa Barbara Basin sediments: Implications for denitrification in the eastern tropical North Pacific during the last 50,000 years. *Paleoceanography* **15**, 377–387 (2000).
66. W. E. Dean, The geochemical record of the last 17,000 years in the Guaymas Basin, Gulf of California. *Chem. Geol.* **232**, 87–98 (2006).
67. H. Cheshire, J. Thurow, A. J. Nederbragt, Late Quaternary climate change record from two long sediment cores from Guaymas Basin, Gulf of California. *J. Quat. Sci.* **20**, 457–469 (2005).
68. T. M. Hill, J. P. Kennett, D. K. Pak, R. J. Behl, C. Robert, L. Beaufort, Pre-Bølling warming in Santa Barbara Basin, California: Surface and intermediate water records of early deglacial warmth. *Quat. Sci. Rev.* **25**, 2835–2845 (2006).

69. A. Shibahara, K. Ohkushi, J. P. Kennett, K. Ikehara, Late Quaternary changes in intermediate water oxygenation and oxygen minimum zone, northern Japan: A benthic foraminiferal perspective. *Paleoceanography* **22**, PA3213 (2007).
70. K. Ikehara, K. Ohkushi, A. Shibahara, M. Hoshiba, Change of bottom water conditions at intermediate depths of the Oyashio region, NW Pacific over the past 20,000 yrs. *Global Planet. Change* **53**, 78–91 (2006).
71. Y. Ishizaki, K. Ohkushi, T. Ito, H. Kawahata, Abrupt changes of intermediate-water oxygen in the northwestern Pacific during the last 27 kyr. *Geo-Mar. Lett.* **29**, 125–131 (2009).
72. O. Cartapanis, K. Tachikawa, E. Bard, Northeastern Pacific oxygen minimum zone variability over the past 70 kyr: Impact of biological production and oceanic ventilation. *Paleoceanography* **26**, PA4208 (2011).
73. M. Shigemitsu, H. Narita, Y. W. Watanabe, N. Harada, S. Tsunogai, Ba, Si, U, Al, Sc, La, Th, C and $^{13}C/^{12}C$ in a sediment core in the western subarctic Pacific as proxies of past biological production. *Mar. Chem.* **106**, 442–455 (2007).
74. Y. Okazaki, K. Takahashi, H. Asahi, K. Katsuki, J. Hori, H. Yasuda, Y. Sagawa, H. Tokuyama, Productivity changes in the Bering Sea during the late Quaternary. *Deep Sea Res. II Top. Stud. Oceanogr.* **52**, 2150–2162 (2005).
75. J. Crusius, T. F. Pedersen, S. E. Calvert, G. L. Cowie, T. Oba, A 36 kyr geochemical record from the Sea of Japan of organic matter flux variations and changes in intermediate water oxygen concentrations. *Paleoceanography* **14**, 248–259 (1999).
76. E. D. Galbraith, S. L. Jaccard, T. F. Pedersen, D. M. Sigman, G. H. Haug, M. Cook, J. R. Southon, R. Francois, Carbon dioxide release from the North Pacific abyss during the last deglaciation. *Nature* **449**, 890–893 (2007).
77. S. L. Jaccard, E. D. Galbraith, D. M. Sigman, G. H. Haug, R. Francois, T. F. Pedersen, P. Dulski, H. R. Thierstein, Subarctic Pacific evidence for a glacial deepening of the oceanic respired carbon pool. *Earth Planet. Sci. Lett.* **277**, 156–165 (2009).
78. E. D. Galbraith, M. Kienast, S. L. Jaccard, T. F. Pedersen, B. G. Brunelle, D. M. Sigman, T. Kiefer, Consistent relationship between global climate and surface nitrate utilization in the western subarctic Pacific throughout the last 500 ka. *Paleoceanography* **23**, PA2212 (2008).

79. S. S. Kienast, S. E. Calvert, T. F. Pedersen, Nitrogen isotope and productivity variations along the northeast Pacific margin over the last 120 kyr: Surface and subsurface paleoceanography. *Paleoceanography* **17**, 1055 (2002).

80. A. C. Mix, D. C. Lund, N. G. Pisias, P. Bodén, L. Bornmalm, M. Lyle, J. Pike, *Rapid Climate Oscillations in the Northeast Pacific During the Last Deglaciation Reflect Northern and Southern Hemisphere Sources* (Geophysical Monograph Series, American Geophysical Union, 1999), vol. 112.

81. J. P. Kennett, B. L. Ingram, A 20,000-year record of ocean circulation and climate change from the Santa Barbara basin. *Nature* **377**, 510–514 (1995).

82. T. Sagawa, K. Ikehara, Intermediate water ventilation change in the subarctic northwest Pacific during the last deglaciation. *Geophys. Res. Lett.* **35**, L24702 (2008).

83. N. Ahagon, K. Ohkushi, M. Uchida, T. Mishima, Mid-depth circulation in the northwest Pacific during the last deglaciation: Evidence from foraminiferal radiocarbon ages. *Geophys. Res. Lett.* **30**, 2097 (2003).

84. M. Hoshiba, N. Ahagon, K. Ohkushi, M. Uchida, I. Motoyama, A. Nishimura, Foraminiferal oxygen and carbon isotopes during the last 34 kyr off northern Japan, northwestern Pacific. *Mar. Micropaleontol.* **61**, 196–208 (2006).

85. M. S. Cook, L. D. Keigwin, Radiocarbon profiles of the NW Pacific from the LGM and deglaciation: Evaluating ventilation metrics and the effect of uncertain surface reservoir ages. *Paleoceanography* **30**, 174–195 (2015).

86. L. D. Keigwin, Late Pleistocene-Holocene paleoceanography and ventilation of the Gulf of California. *J. Oceanogr.* **58**, 421–432 (2002).

87. H. Gebhardt, M. Sarnthein, P. M. Grootes, T. Kiefer, H. Kuehn, F. Schmieder, U. Röhl, Paleonutrient and productivity records from the subarctic North Pacific for Pleistocene glacial terminations I to V. *Paleoceanography* **23**, PA4212 (2008).

88. S. A. Gorbarenko, J. R. Southon, L. D. Keigwin, M. V. Cherepanova, I. G. Gvozdeva, Late Pleistocene–Holocene oceanographic variability in the Okhotsk Sea: Geochemical, lithological and paleontological evidence. *Palaeogeogr. Palaeoclimatol. Palaeoecol.* **209**, 281–301 (2004).

89. D. C. Lund, A. C. Mix, J. Southon, Increased ventilation age of the deep northeast Pacific Ocean during the last deglaciation. *Nat. Geosci.* **4**, 771–774 (2011).

90. J.-C. Duplessy, M. Arnold, E. Bard, A. Juillet-Leclerc, N. Kallel, L. Labeyrie, AMS ^{14}C study of transient events and of the ventilation rate of the Pacific intermediate water during the last deglaciation. *Radiocarbon* **31**, 493–502 (1989).
91. K. Minoshima, H. Kawahata, T. Irino, K. Ikehara, K. Aoki, M. Uchida, M. Yoneda, Y. Shibata, Deep water ventilation in the northwestern North Pacific during the last deglaciation and the early Holocene (15-5 cal. kyr B.P.) based on AMS ^{14}C dating. *Nucl. Instrum. Methods Phys. Res. Sect. B* **259**, 448–452 (2007).
92. A. VanGeen, R. G. Fairbanks, P. Dartnell, M. McGann, J. V. Gardner, M. Kashgarian, Ventilation changes in the northeast Pacific during the Last Deglaciation. *Paleoceanography* **11**, 519–528 (1996).
93. K. Ikehara, T. Danhara, T. Yamashita, M. Tanahashi, S. Morita, K. Ohkushi, Paleoceanographic control on a large marine reservoir effect offshore of Tokai, south of Japan, NW Pacific, during the last glacial maximum-deglaciation. *Quat. Int.* **246**, 213–221 (2011).
94. P. A. Rafter, J.-C. Herguera, J. R. Southon, Extreme lowering of deglacial seawater radiocarbon recorded by both epifaunal and infaunal benthic foraminifera in a wood-dated sediment core. *Clim. Past* **14**, 1977–1989 (2018).
95. M. Sarnthein, P. M. Grootes, J. P. Kennett, M.-J. Nadeau, ^{14}C reservoir ages show deglacial changes in ocean currents and carbon cycle, in *Ocean Circulation: Mechanisms and Impacts—Past and Future Changes of Meridional Overturning* (Geophysical Monograph Series, American Geophysical Union, 2007), vol. 173, pp. 175–196.
96. S. Wan, Z. Jian, Deep water exchanges between the South China Sea and the Pacific since the last glacial period. *Paleoceanography* **29**, 1162–1178 (2014).
97. M. Sarnthein, S. Balmer, P. M. Grootes, M. Mudelsee, Planktic and benthic ^{14}C reservoir ages for three ocean basins, calibrated by a suite of ^{14}C Plateaus in the glacial-to-deglacial Suigetsu atmospheric ^{14}C record. *Radiocarbon* **57**, 129–151 (2016).
98. Y. Okazaki, K. Kimoto, H. Asahi, M. Sato, Y. Nakamura, N. Harada, Glacial to deglacial ventilation and productivity changes in the southern Okhotsk Sea. *Palaeogeogr. Palaeoclimatol. Palaeoecol.* **395**, 53–66 (2014).
99. S. C. Bova, T. D. Herbert, M. A. Altabet, Ventilation of northern and southern sources of aged carbon in the eastern equatorial Pacific during the younger dryas rise in atmospheric CO_2. *Paleoceanogr. Paleoclimatol.* **33**, 1151–1168 (2018).

100. C. M. Lindsay, S. J. Lehman, T. M. Marchitto, J. D. Carriquiry, J. D. Ortiz, New constraints on deglacial marine radiocarbon anomalies from a depth transect near Baja California. *Paleoceanography* **31**, 1103–1116 (2016).

101. A. Olsen, R. M. Key, S. Van Heuven, S. K. Lauvset, A. Velo, X. Lin, C. Schirnick, A. Kozyr, T. Tanhua, M. Hoppema, S. Jutterström, The Global Ocean Data Analysis Project version 2 (GLODAPv2)–an internally consistent data product for the world ocean. *Earth Syst. Sci. Data* **8**, (2016).

102. P. J. Reimer, E. Bard, A. Bayliss, J. W. Beck, P. G. Blackwell, C. B. Ramsey, C. E. Buck, H. Cheng, R. L. Edwards, M. Friedrich, P. M. Grootes, T. P. Guilderson, H. Haflidason, I. Hajdas, C. Hatté, T. J. Heaton, D. L. Hoffmann, A. G. Hogg, K. A. Hughen, K. F. Kaiser, B. Kromer, S. W. Manning, M. Niu, R. W. Reimer, D. A. Richards, E. M. Scott, J. R. Southon, R. A. Staff, C. S. M. Turney, J. van der Plicht, IntCal13 and Marine13 radiocarbon age calibration curves 0–50,000 years cal BP. *Radiocarbon* **55**, 1869–1887 (2013).

103. H. Kawahata, K.-i. Ohkushi, Y. Hatakeyama, Comparative Late Pleistocene paleoceanographic changes in the mid latitude boreal and austral western Pacific. *J. Oceanogr.* **55**, 747–761 (1999).

104. L. Maeda, H. Kawahata, M. Nohara, Fluctuation of biogenic and abiogenic sedimentation on the Shatsky Rise in the western North Pacific during the late Quaternary. *Mar. Geol.* **189**, 197–214 (2002).

105. I. L. Hendy, T. F. Pedersen, J. P. Kennett, R. Tada, Intermittent existence of a southern Californian upwelling cell during submillennial climate change of the last 60 kyr. *Paleoceanography* **19** (2004).

106. H. Kawahata, A. Suzuki, H. Ohta, Export fluxes in the Western Pacific Warm Pool. *Deep Sea Res. I Oceanogr. Res. Pap.* **47**, 2061–2091 (2000).

107. R. S. Ganeshram, T. F. Pedersen, Glacial-interglacial variability in upwelling and bioproductivity off NW Mexico: Implications for Quaternary paleoclimate. *Paleoceanography* **13**, 634–645 (1998).

108. L. D. Keigwin, G. A. Jones, P. N. Froelich, A 15,000 year paleoenvironmental record from Meiji Seamount, far northwestern Pacific. *Earth Planet. Sci. Lett.* **111**, 425–440 (1992).

109. S. A. Gorbarenko, Stable isotope and lithologic evidence of late-glacial and Holocene oceanography of the Northwestern Pacific and its marginal seas. *Quatern. Res.* **46**, 230–250 (1996).

110. B. G. Brunelle, D. M. Sigman, S. L. Jaccard, L. D. Keigwin, B. Plessen, G. Schettler, M. S. Cook, G. H. Haug, Glacial/interglacial changes in nutrient supply and stratification in the western subarctic North Pacific since the penultimate glacial maximum. *Quat. Sci. Rev.* **29**, 2579–2590 (2010).

111. Y. Okazaki, K. Takahashi, K. Katsuki, A. Ono, J. Hori, T. Sakamoto, M. Uchida, Y. Shibata, M. Ikehara, K. Aoki, Late Quaternary paleoceanographic changes in the southwestern Okhotsk Sea: Evidence from geochemical, radiolarian, and diatom records. *Deep Sea Res. II Top. Stud. Oceanogr.* **52**, 2332–2350 (2005).

112. K. Minoshima, H. Kawahata, K. Ikehara, Changes in biological production in the mixed water region (MWR) of the northwestern North Pacific during the last 27 kyr. *Palaeogeogr. Palaeoclimatol. Palaeoecol.* **254**, 430–447 (2007).

113. O. Seki, M. Ikehara, K. Kawamura, T. Nakatsuka, K. Ohnishi, M. Wakatsuchi, H. Narita, T. Sakamoto, Reconstruction of paleoproductivity in the Sea of Okhotsk over the last 30 kyr. *Paleoceanography* **19**, PA1016 (2004).

114. H. Narita, M. Sato, S. Tsunogai, M. Murayama, M. Ikehara, T. Nakatsuka, M. Wakatsuchi, N. Harada, Y. Ujiié, Biogenic opal indicating less productive northwestern North Pacific during the glacial ages. *Geophys. Res. Lett.* **29**, 22–1–22–4 (2002).

115. S. A. Gorbarenko, E. L. Goldberg, M. Kashgarian, T. A. Velivetskaya, S. P. Zakharkov, V. S. Pechnikov, A. A. Bosin, O. Y. Psheneva, E. D. Ivanova, Millennium scale environment changes of the Okhotsk Sea during last 80 kyr and their phase relationship with global climate changes. *J. Oceanogr.* **63**, 609–623 (2007).

116. S. A. Gorbarenko, T. A. Khusid, I. A. Basov, T. Oba, J. R. Southon, I. Koizumi, Glacial Holocene environment of the southeastern Okhotsk Sea: Evidence from geochemical and palaeontological data. *Palaeogeogr. Palaeoclimatol. Palaeoecol.* **177**, 237–263 (2002).

117. D. Nürnberg, R. Tiedemann, Environmental change in the Sea of Okhotsk during the last 1.1 million years. *Paleoceanography* **19**, PA4011 (2004).

118. B. G. Brunelle, D. M. Sigman, M. S. Cook, L. D. Keigwin, G. H. Haug, B. Plessen, G. Schettler, S. L. Jaccard, Evidence from diatom-bound nitrogen isotopes for subarctic Pacific stratification during the last ice age and a link to North Pacific denitrification changes. *Paleoceanography* **22**, PA1215 (2007).

119. E. Maier, M. Méheust, A. Abelmann, R. Gersonde, B. Chapligin, J. Ren, R. Stein, H. Meyer, R. Tiedemann, Deglacial subarctic Pacific surface water hydrography and nutrient dynamics and links to North Atlantic climate variability and atmospheric CO_2. *Paleoceanography* **30**, 949–968 (2015).

120. P. J. Lam, L. F. Robinson, J. Blusztajn, C. Li, M. S. Cook, J. F. McManus, L. D. Keigwin, Transient stratification as the cause of the North Pacific productivity spike during deglaciation. *Nat. Geosci.* **6**, 622–626 (2013).
121. K. P. Knudson, A. C. Ravelo, Enhanced subarctic Pacific stratification and nutrient utilization during glacials over the last 1.2 Myr. *Geophys. Res. Lett.* **42**, 9870–9879 (2015).
122. S. Kim, K. Takahashi, B.-K. Khim, Y. Kanematsu, H. Asahi, A. C. Ravelo, Biogenic opal production changes during the Mid-Pleistocene Transition in the Bering Sea (IODP Expedition 323 Site U1343). *Quatern. Res.* **81**, 151–157 (2014).
123. L. Rodríguez Sanz, P. G. Mortyn, J. C. Herguera, R. Zahn, Hydrographic changes in the tropical and extratropical Pacific during the last deglaciation. *Paleoceanography* **28**, 529–538 (2013).
124. M. A. Taylor, I. L. Hendy, D. K. Pak, Deglacial ocean warming and marine margin retreat of the Cordilleran Ice Sheet in the North Pacific Ocean. *Earth Planet. Sci. Lett.* **403**, 89–98 (2014).
125. T. Sagawa, K. Toyoda, T. Oba, Sea surface temperature record off central Japan since the Last Glacial Maximum using planktonic foraminiferal Mg/Ca thermometry. *J. Quat. Sci.* **21**, 63–73 (2005).
126. D. K. Pak, D. W. Lea, J. P. Kennett, Millennial scale changes in sea surface temperature and ocean circulation in the northeast Pacific, 10–60 kyr BP. *Paleoceanography* **27**, PA1212 (2012).
127. Y. Kubota, K. Kimoto, R. Tada, H. Oda, Y. Yokoyama, H. Matsuzaki, Variations of East Asian summer monsoon since the last deglaciation based on Mg/Ca and oxygen isotope of planktic foraminifera in the northern East China Sea. *Paleoceanography* **25**, PA4205 (2010).
128. N. Harada, N. Ahagon, M. Uchida, M. Murayama, Northward and southward migrations of frontal zones during the past 40 kyr in the Kuroshio-Oyashio transition area. *Geochem. Geophys. Geosyst.* **5**, Q09004 (2004).
129. N. Harada, M. Sato, A. Shiraishi, M. C. Honda, Characteristics of alkenone distributions in suspended and sinking particles in the northwestern North Pacific. *Geochim. Cosmochim.* **70**, 2045–2062 (2006).
130. N. Harada, M. Sato, T. Sakamoto, Freshwater impacts recorded in tetraunsaturated alkenones and alkenone sea surface temperatures from the Okhotsk Sea across millennial-scale cycles. *Paleoceanography* **23**, PA3201 (2008).

131. M. Inagaki, M. Yamamoto, Y. Igarashi, K. Ikehara, Biomarker records from core GH02-1030 off Tokachi in the northwestern Pacific over the last 23,000 years: Environmental changes during the last deglaciation. *J. Oceanogr.* **65**, 847–858 (2009).

132. T. D. Herbert, J. D. Schuffert, D. Andreasen, L. Heusser, M. Lyle, A. Mix, A. C. Ravelo, L. D. Stott, J. C. Herguera, Collapse of the California current during Glacial Maxima linked to climate change on land. *Science* **293**, 71–76 (2001).

133. K. Sawada, N. Handa, Variability of the path of the Kuroshio ocean current over the past 25,000 years. *Nature* **392**, 592–595 (1998).

134. M. Yamamoto, T. Oba, J. Shimamune, T. Ueshima, Orbital-scale anti-phase variation of sea surface temperature in mid-latitude North Pacific margins during the last 145,000 years. *Geophys. Res. Lett.* **31**, L16311 (2004).

135. D. Isono, M. Yamamoto, T. Irino, T. Oba, M. Murayama, T. Nakamura, H. Kawahata, The 1500-year climate oscillation in the midlatitude North Pacific during the Holocene. *Geology* **37**, 591–594 (2009).

136. W. R. Gray, D. Evans, Nonthermal influences on Mg/Ca in planktonic foraminifera: A review of culture studies and application to the last glacial maximum. *Paleoceanogr. Paleoclimatol.* **34**, 306–315 (2019).

137. J. E. Tierney, S. B. Malevich, W. Gray, L. Vetter, K. Thirumalai, Bayesian calibration of the Mg/Ca paleothermometer in planktic foraminifera. *Paleoceanogr. Paleoclimatol.* **34**, 2005–2030 (2019).

138. W. R. Gray, S. Weldeab, D. W. Lea, Y. Rosenthal, N. Gruber, B. Donner, G. Fischer, The effects of temperature, salinity, and the carbonate system on Mg/Ca in *Globigerinoides ruber* (white): A global sediment trap calibration. *Earth Planet. Sci. Lett.* **482**, 607–620 (2018).

139. M. Regenberg, A. Regenberg, D. Garbe-Schönberg, D. W. Lea, Global dissolution effects on planktonic foraminiferal Mg/Ca ratios controlled by the calcite-saturation state of bottom waters. *Paleoceanography* **29**, 127–142 (2014).

140. J. Yu, R. F. Anderson, Z. Jin, J. W. B. Rae, B. N. Opdyke, S. M. Eggins, Responses of the deep ocean carbonate system to carbon reorganization during the Last Glacial–interglacial cycle. *Quat. Sci. Rev.* **76**, 39–52 (2013).

141. F. G. Prahl, L. A. Muehlhausen, D. L. Zahnle, Further evaluation of long-chain alkenones as indicators of paleoceanographic conditions. *Geochim. Cosmochim. Acta* **52**, 2303–2310 (1988).

142. M. H. Conte, M.-A. Sicre, C. Rühlemann, J. C. Weber, S. Schulte, D. Schulz-Bull, T. Blanz, Global temperature calibration of the alkenone unsaturation index ($U^{K'}_{37}$) in surface waters and comparison with surface sediments. *Geochem. Geophys. Geosyst.* **7**, Q02005 (2006).

143. J. E. Tierney, M. P. Tingley, BAYSPLINE: A new calibration for the alkenone paleothermometer. *Paleoceanogr. Paleoclimatol.* **33**, 281–301 (2018).

144. S.-T. Kim, J. R. O'Neil, Equilibrium and nonequilibrium oxygen isotope effects in synthetic carbonates. *Geochim. Cosmochim. Acta* **61**, 3461–3475 (1997).

145. J. F. Adkins, K. McIntyre, D. P. Schrag, The salinity, temperature, and $\delta^{18}O$ of the glacial deep ocean. *Science* **298**, 1769–1773 (2002).

146. K. Lambeck, H. Rouby, A. Purcell, Y. Sun, M. Sambridge, Sea level and global ice volumes from the Last Glacial Maximum to the Holocene. *Proc. Natl. Acad. Sci. U.S.A.* **111**, 15296–15303 (2014).

147. S. A. Marcott, J. D. Shakun, P. U. Clark, A. C. Mix, A reconstruction of regional and global temperature for the past 11,300 years. *Science* **339**, 1198–1201 (2013).

148. R. C. Wills, T. Schneider, Stationary eddies and the zonal asymmetry of net precipitation and ocean freshwater forcing. *J. Climate* **28**, 5115–5133 (2015).

149. R. Schlitzer, *Ocean Data View* (Alfred Wegener Institute for Polar and Marine Research, 2004).

150. L. Cao, M. Eby, A. Ridgwell, K. Caldeira, D. Archer, A. Ishida, F. Joos, K. Matsumoto, U. Mikolajewicz, A. Mouchet, J. C. Orr, G.-K. Plattner, R. Schlitzer, K. Tokos, I. Totterdell, T. Tschumi, Y. Yamanaka, A. Yool, The role of ocean transport in the uptake of anthropogenic CO_2. *Biogeosciences* **6**, 375–390 (2009).

151. A. Ridgwell, I. Zondervan, J. C. Hargreaves, J. Bijma, T. M. Lenton, Assessing the potential long-term increase of oceanic fossil fuel CO_2 uptake due to CO_2-calcification feedback. *Biogeosciences* **4**, 481–492 (2007).

152. A. Tagliabue, O. Aumont, R. DeAth, J. P. Dunne, S. Dutkiewicz, E. Galbraith, K. Misumi, J. K. Moore, A. Ridgwell, E. Sherman, C. Stock, M. Vichi, C. Völker, A. Yool, How well do global ocean biogeochemistry models simulate dissolved iron distributions? GBC, 10.1002/2015GB005289 (2016).

153. L. Loulergue, A. Schilt, R. Spahni, V. Masson-Delmotte, T. Blunier, B. Lemieux, J.-M. Barnola, D. Raynaud, T. F. Stocker, J. Chappellaz, Orbital and millennial-scale features of atmospheric CH4 over the past 800,000 years. *Nature* **453**, 383–386 (2008).

154. E. Monnin, A. Indermühle, A. Dällenbach, J. Flückiger, B. Stauffer, T. F. Stocker, D. Raynaud, J.-M. Barnola, Atmospheric CO2 concentrations over the last glacial termination. *Science* **291**, 112–114 (2001).

155. A. Schilt, M. Baumgartner, J. Schwander, D. Buiron, E. Capron, J. Chappellaz, L. Loulergue, S. Schüpbach, R. Spahni, H. Fischer, T. F. Stocker, Atmospheric nitrous oxide during the last 140,000 years. *Earth Planet. Sci. Lett.* **300**, 33–43 (2010).

156. R. Marsh, A. Yool, T. M. Lenton, M. Y. Gulamali, N. R. Edwards, J. G. Shepherd, M. Krznaric, S. Newhouse, S. J. Cox, Bistability of the thermohaline circulation identified through comprehensive 2-parameter sweeps of an efficient climate model. *Climate Dynamics* **23**, 761–777 (2004).

157. N. R. Edwards, R. Marsh, Uncertainties due to transport-parameter sensitivity in an efficient 3-D ocean-climate model. *Climate Dynamics* **24**, 415–433 (2005).

158. J. W. B. Rae, W. S. Broecker, What fraction of the Pacific and Indian oceans' deep water is formed in the Southern Ocean? *Biogeosciences* **15**, 3779–3794 (2018).

159. N. Ducet, P. Y. Le Traon, Global high-resolution mapping of ocean circulation from TOPEX/Poseidon and ERS-1 and -2. *J. Geophys. Res.* **105**, 19477–19498 (2000).

160. T. M. Marchitto, W. B. Curry, J. Lynch-Stieglitz, S. P. Bryan, K. M. Cobb, D. C. Lund, Improved oxygen isotope temperature calibrations for cosmopolitan benthic foraminifera. *Geochim. Cosmochim. Acta* **130**, 1–11 (2014).

161. S. N. Wood, Fast stable restricted maximum likelihood and marginal likelihood estimation of semiparametric generalized linear models. *J. R. Stat. Soc. Ser. B* **73**, 3–36 (2011).

162. A. Schmittner, N. Gruber, A. C. Mix, R. M. Key, A. Tagliabue, T. K. Westberry, Biology and air-sea gas exchange controls on the distribution of carbon isotope ratios ($\delta^{13}C$) in the ocean. *Biogeosciences* **10**, 5793–5816 (2013).

163. G. L. Simpson, Modelling palaeoecological time series using generalised additive models. *Front. Ecol. Evol.* **6**, 149 (2018).

164. B. L. Otto-Bliesner, E. C. Brady, G. Clauzet, R. Tomas, S. Levis, Z. Kothavala, Last Glacial Maximum and Holocene climate in CCSM3. *J. Climate* **19**, 2526–2544 (2006).

165. I. Eisenman, C. M. Bitz, E. Tziperman, Rain driven by receding ice sheets as a cause of past climate change. *Paleoceanography* **24**, PA4209 (2009).

166. W. R. Peltier, Global glacial isostasy and the surface of the ice-age Earth: The ICE-5G (VM2) model and Grace. *Annu. Rev. Earth Planet. Sci.* **32**, 111–149 (2004).

167. E. Galbraith, C. de Lavergne, Response of a comprehensive climate model to a broad range of external forcings: Relevance for deep ocean ventilation and the development of late Cenozoic ice ages. *Climate Dynam.* **52**, 653–679 (2019).

168. R. F. Ivanovic, L. J. Gregoire, M. Kageyama, D. M. Roche, P. J. Valdes, A. Burke, R. Drummond, W. R. Peltier, L. Tarasov, Transient climate simulations of the deglaciation 21–9 thousand years before present (version 1) – PMIP4 Core experiment design and boundary conditions. *Geosci. Model Dev.* **9**, 2563–2587 (2016).